



# Smart microgels as drug delivery vehicles for the natural drug aescin: uptake, release and interactions

Maxim Dirksen<sup>1</sup> · Carina Dargel<sup>1</sup> · Lukas Meier<sup>1</sup> · Timo Brändel<sup>2,3</sup> · Thomas Hellweg<sup>1</sup>

Received: 21 January 2020 / Revised: 19 February 2020 / Accepted: 26 February 2020 / Published online: 22 March 2020  
© The Author(s) 2020

## Abstract

In the present study, we show how acrylamide-based microgels can be employed for the uptake and release of the drug  $\beta$ -aescin, a widely used natural product with a variety of pharmacological effects. We show how aescin is incorporated into the microgel particles. It has an important influence on the structure of the microgels, by reducing their natural network-density gradient in the swollen state. Moreover, temperature-dependent measurements reveal how the incorporation of aescin stabilizes the microgel particles, while the volume phase transition temperature (VPPT) is almost constant, which is very important for the intended drug release. Finally, it is shown that upon increase of the temperature above the VPPT the particles are able to release aescin from their network, encouraging the use of this particular drug delivery system for hypothermia treatments.

**Keywords** Microgels · Drug delivery · Biosurfactants · Saponins · Aescin

## Introduction

Nowadays, stimuli-responsive microgels are investigated as potential candidates for a lot of applications in many different fields ranging from catalytic microreactors to cell culture substrates [1, 2]. One of the most promising ideas for a possible biomedical application of microgels has always been their use as drug delivery systems. In recent years, drug release has become increasingly important in human medicine and the health sector [3–5]. Here, the main aim is the targeted release of active ingredients while the bio-availability is maintained, thus preventing the premature degradation of the drug. In addition, targeted release of the required amount of the drug minimizes side effects in other regions of the body which should not be treated. For this purpose, synthetic polymers are becoming more

interesting as therapeutic agents, since these usually show better pharmacokinetics compared with small molecule drugs due to longer circulation time [4, 6–8].

In this particular context, stimuli-responsive hydrogels have been examined as promising candidates [2, 9, 10] in detail during the past decades concerning their uptake and release ability of different kinds of molecules [11, 12]. Besides ibuprofen and other drugs, also many surfactants were investigated due to their tunable interactions with microgel particles [13–17]. For instance, Tam et al. [18] investigated the uptake and release of nonionic PEO-based surfactants inside poly-*N*-isopropylacrylamide (PNIPAM) microgels. They deduced that these cross-linked polymer particles are excellent candidates for the uptake of surfactant-like structures due to their ability to bind them in their sponge-like interior. Moreover, PNIPAM-based microgels exhibit a structure, which is energetically favorable for the assembly with surfactants. Due to the synthesis by precipitation polymerization introduced by Pelton et al. [19], PNIPAM microgel particles have a rather high number of surface charges. These surface charges result from the charged initiator. The particle center is rather polymer rich, because of a cross-linker gradient from the inside to the outside of the particle [20]. Hence, microgels exhibit regions, with favorable interactions with both parts of the surfactants, the hydrophilic part of the particle surface, and the hydrophobic part in the particle interior.

✉ Thomas Hellweg  
thomas.hellweg@uni-bielefeld.de

<sup>1</sup> Department of Physical and Biophysical Chemistry, Bielefeld University, Universitätsstrasse 25, 33615, Bielefeld, Germany

<sup>2</sup> Donostia International Physics Center, Paseo Manuel de Lardizabal 4, 20018, San Sebastian, Spain

<sup>3</sup> Centro de Física de Materiales (CFM) (CSIC-UPV/EHU), Materials Physics Center (MPC), Paseo Manuel de Lardizabal 5, 20018, San Sebastian, Spain

Besides the mentioned structure, the most remarkable property of PNIPAM microgels is their ability to respond to a change in temperature with a considerable change in size, without losing colloidal stability [21]. The size change is driven by a microphase separation of the single polymer chains, when the lower critical solution temperature (LCST) of PNIPAM is crossed. This transition exhibits a rather continuous shape, which is probably due to the variability of chain lengths inside the polymer network [19]. Therefore, the characteristic temperature of the particle size-change is usually not called LCST but rather volume phase transition temperature (VPTT). Typical PNIPAM microgels exhibit a VPTT of 33 °C [22], which unfortunately diminishes their real applicability as drug carriers, if the human body temperature of around 37 °C is taken into account. Practically, another well-studied microgel system consisting of poly-*N*-isopropylmethacrylamide (PNIPMAM) exhibits a much higher VPTT of around 44 °C [23]. However, the basic principle behind all studies introducing stimuli-responsive microgels as drug delivery materials is to make use of this outstanding phase transition behavior by encapsulating drugs in either the swollen or collapsed state and afterwards releasing the drug by crossing the VPTT in the respective direction [12].

The present study focuses on the uptake and release of the natural drug  $\beta$ -aescin performing the uptake of the drug in the swollen state and triggering its release by heating up the system above the VPTT.  $\beta$ -Aescin is a natural surfactant belonging to the group of saponins and can be assigned to the family of glycosidic compounds [24, 25] present in many plants. Saponins are used in a variety of areas like cosmetics [26], pharmaceuticals [27], or agriculture [28]. The structure of saponins consists of a triterpenic or steroidal backbone linked to a glycosidic moiety [29–31]. Therewith, saponins possess well-separated hydrophobic as well as hydrophilic moieties and are natural surfactants. It was shown in several studies that saponins have anti-inflammatory properties [32, 33] and are able to cause different physiological effects in the human body [34–37]. Many of these effects are thought to be based on the mentioned amphiphilic structure, but the origin of these effects is not completely clear at the moment.

Because of that, a series of investigations has been performed on the saponin  $\beta$ -aescin [38], which can be extracted from the horse chestnut tree *Aesculus hippocastanum* [39–43]. These natural aescin extracts contain a mixture of several substances, which are similar in their structure and modifications can mostly be found in the kind of sugars attached and in the location of the residues on the triterpenic backbone. However, the aescin purchased from Sigma-Aldrich (Munich, Germany) and used in the mentioned publications is a mixture of basically two substances. The molecular structure of these substances is shown in

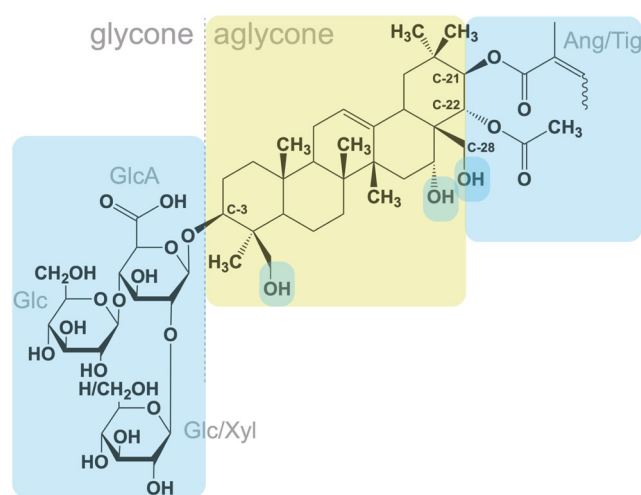


**Fig. 1** Lewis-structure of two main components present in the aescin mixture used in this study. The two structures are cis-trans-isomers and only differ in the acid attached to the C-21 position of the triterpenic backbone (indicated by an indeterminate bond). Hydrophilic regions of the molecule are marked with blue boxes; hydrophobic moieties are marked with yellowish color

Fig. 1 and both substances are cis-trans-isomers differing in the acid attached to the C-21 position, which is either tiglic or angelic acid (see indeterminate bond in Fig. 1). The structure of aescin can be compared with the one of bile salts, which are also based on a rigid and cyclic backbone with several small hydrophilic groups attached. Due to the comparably large sugar residue, aescin possesses a much better defined hydrophilic group. Nevertheless, the action of aescin concerning the interaction with lipid membranes is similar to the one of bile salts [44–46]. The interaction of aescin with model membranes composed of the phospholipid 1,2-dimyristoyl-*sn*-glycero-3-phosphocholine (DMPC) has been reviewed recently by Geisler et al. [47]. The ability to incorporate into the lipid bilayer changes, e.g., the membrane elasticity and moreover induces aggregation effects. Finally, at sufficiently high aescin concentration, the membrane is completely solubilized and smaller, bicellar structures build by a continuous lipid bilayer rim-stabilized by aescin molecules are formed. These experiments directly proved that aescin acts like a surfactant. Additionally, Dargel et al. [38] investigated the self-assembly process of  $\beta$ -aescin and were able to determine its critical micellar concentration (*cmc*) to a concentration of 0.35 mM in a 50 mM phosphate buffer with a physiological pH value of 7.4. This rather low *cmc* shows that the influence of the triterpenic backbone is very pronounced and  $\beta$ -aescin has to be considered as rather hydrophobic.

Keeping the abovementioned physiological functions, the structural properties, and the self-assembly conditions in mind, it seems straightforward to develop a method for a successful delivery of aescin into the human body in the next

step. To the best of our knowledge, such a carrier system was not characterized so far. Hence, it is unknown which properties of a carrier system are required for a sufficient uptake and release of aescin. Since microgels, as mentioned before, have been extensively studied concerning this possible application, it is natural to begin the development with the same approach performed for many other drugs before.

Consequently, we investigated PNIPAM and PNIPMAM microgels with respect to their general ability to take up aescin concentrations around the *cmc*. The *cmc* is, based on Dargel et al. [38], a concentration of 0.35 mM and aescin concentrations are given related to this value. Furthermore, we investigated the influence of the incorporation of these different amounts of aescin, namely 25%, 50%, 75%, and 175% of the *cmc*, on the particle structure and swelling behavior and their colloidal stability using atomic force microscopy (AFM), static light scattering (SLS), and photon correlation spectroscopy (PCS). To get insight into the swelling behavior of the microgel particles, we measured the swelling curves of the microgel particles and fitted them with a sigmoidal function to obtain the VPTT as the inflection point of the curves. In this way, the effect of the aescin uptake on the VPTT of PNIPAM and PNIPMAM microgels can be compared independently. Finally, we investigated the triggered release of aescin by means of UV/Vis measurements.

## Materials and methods

### Materials

If not indicated differently, all chemicals were purchased from Sigma Aldrich, Munich, Germany. *N*-Isopropylacrylamide (NIPAM, TCI Germany GmbH, Eschborn, Germany; 97%) and *N*-isopropylmethacrylamide (NIPMAM, 97%) were recrystallized from *n*-hexane (p.a., VWR International, Eschborn, Germany). *N,N'*-methylenebis-acrylamide (BIS, 99%), sodium dodecyl sulfate (SDS, 99%), ammonium persulfate (APS, 99%), polyethylene-imine (PEI, branched 99%), and the saponin aescin ( $\geq 95\%$ , CAS number 6805-41-0) were used without further purification. Water was purified using an Arium pro VF system (Satorius AG, Göttingen, Germany).

### Microgel synthesis

The microgels were synthesized via the classical Pelton [19] synthesis approach. For both syntheses, the monomers NIPAM (11.55 mmol) or NIPMAM (11.55 mmol) and BIS (0.577 mmol, 5 mol%) were dissolved in 74 mL purified water. The solution was heated by an oil bath (80 °C) under continuous stirring (400 rpm) and purged with nitrogen for

1 h. Ten minutes before the polymerization was initiated, different amounts of SDS (2.5 mmol for NIPAM, 1.5 mmol for NIPMAM) were added. The polymerization was initiated by the addition of APS (0.41 mmol, 3.5 mol%) dissolved in 1 mL purified water and proceeded for 4 h under constant stirring at an oil bath temperature of 80 °C. Afterwards, the reaction mixture was cooled down to room temperature and stirred overnight. The microgels were purified by five consecutive centrifugation (20 000 rpm, 45 min), decantation, and redispersion cycles with purified water.

### Investigation of the aescin uptake and release

The uptake of aescin was investigated using an Agilent 8453 UV/Vis spectrometer (Agilent Technologies Germany, Ratingen, Germany) equipped with a diode-array detector. The sample holder was thermalized to 20 °C, controlled by a water thermostat (Haake Phoenix II, Thermo Haake GmbH, Mühlheim, Germany). For the sample preparation, solutions consisting of a constant microgel amount (0.02 wt%) and different aescin concentrations (0.1 mM–0.7 mM; molar ratio = 0.006–0.014 related to one repeating unit of the polymer (100 monomer units)) with a total volume of 1 mL were centrifuged for 30 min (15000 rpm) using a Mikro 200R centrifuge (Andreas Hettich GmbH & Co. KG, Tuttlingen, Germany). The supernatant was completely removed and replaced by the same amount of purified water. In addition, a microgel sample without aescin was prepared using the same procedure. The solutions were transferred in Hellma cuvettes (Hellma GmbH, Müllheim, Germany, 1 mm) and equilibrated for 25 min. The absorption was measured from 190 to 440 nm.

The same setup was used to study the release of aescin. For the sample preparation, solutions of a constant microgel amount (0.5 wt%) and an aescin concentration of 0.7 mM (molar ratio = 0.016 related to one repeating unit of the polymer (100 monomer units)) with a total volume of 1 mL were centrifuged for 30 min (15000 rpm). The supernatant was completely removed, replaced by the same amount of purified water, and centrifuged again for 30 min (15000 rpm) at temperatures of 10 °C and 50 °C respectively. The supernatants were transferred in a Hellma cuvette (Hellma GmbH, Müllheim, Germany, 1 mm). The absorption was measured from 190 to 440 nm.

### Photon correlation spectroscopy

For the sample preparation, suspensions with a constant microgel concentration ( $c_{MG} = 0.002$  wt%) and  $\beta$ -aescin concentrations of 0 mM, 0.1 mM, 0.2 mM, 0.3 mM, and 0.7 mM were prepared by dilution with a phosphate buffer (pH = 7). In addition, the respective microgels were also highly diluted with purified water.

To determine the particle size, angle-dependent measurements were performed using a 3D-LS Spectrometer Pro (LS Instruments AG, Fribourg, Switzerland) equipped with a HeNe LASER (JDSU 1145P, Thorlabs Inc., Newton, NJ, USA). The temperature was adjusted to 10 °C and 50 °C using a thermostated index matching bath with an equilibration time of 20 min for each temperature. Three measurements were executed at each angle in a range of 30 to 120° in 5° increments.

To investigate the temperature-dependent phase behavior and the volume phase transition temperature (VPTT), a setup with a HeNe LASER (HNL210L, Thorlabs Inc., Newton, NJ, USA) with an ALV-6010 multiple- $\tau$  correlator (ALV GmbH, Langen, Germany) at a constant scattering angle of 60° was used. The temperature was adjusted using a thermostated index matching bath. The measurements were performed in a temperature range of 10 to 60 °C. At each temperature, the sample was allowed to equilibrate for 25 min. The temperature-dependent measurements were used to obtain the swelling curves of the microgels (hydrodynamic radius vs. temperature) and to determine the VPTT.

The resulting auto-correlation functions were analyzed using the methods of cumulants [48] and CONTIN [49] to obtain the mean relaxation rates  $\bar{\Gamma}$  which were plotted against the square of the magnitude of the scattering vector  $q^2$ . The translational diffusion coefficient  $D_T$  can be calculated from the linear dependency of  $\bar{\Gamma}$  on  $q^2$  (see Eq. 1)

$$\bar{\Gamma} = D_T \cdot q^2 \quad (1)$$

with

$$q = |\vec{q}| = \frac{4\pi n}{\lambda} \sin\left(\frac{\theta}{2}\right) \quad (2)$$

Here,  $\lambda$  is the wavelength of the scattered light,  $n$  the refractive index of the solvent, and  $\theta$  the scattering angle. Using the Stokes-Einstein equation (Eq. 3) with the temperature  $T$ , the Boltzmann constant  $k_b$ , and the dynamic solvent viscosity  $\eta$ , a calculation of the hydrodynamic radius  $R_h$  of the microgel particles is possible:

$$D_T = \frac{k_b T}{6\pi \eta R_h} \quad (3)$$

### Static light scattering

All samples (see “Photon correlation spectroscopy”) were used for SLS measurements at 10 °C on a 3D-LS spectrometer (see “Photon correlation spectroscopy”). To normalize the scattering intensity to absolute values, Eq. 4 was used.

$$I_{abs,\theta} = \frac{I_{s,\theta} - I_{sol,\theta}}{I_{tol,\theta}} \cdot R_{tol} \cdot \left(\frac{n_{sol}}{n_{tol}}\right)^2 \quad (4)$$

Here,  $I_{s,\theta}$  is the sample scattering intensity at the angle  $\theta$ ,  $I_{sol,\theta}$  the respective solvent scattering intensity, and  $n_{sol}$  is the refractive index of the solvent. Toluene was used as standard with the Rayleigh ratio  $R_{tol}$ , the refractive index  $n_{tol}$ , and the scattering intensity  $I_{tol,\theta}$ . For the calculation of the radius of gyration  $R_g$  of the microgel particles, a Guinier analysis of the scattering data was performed with a linear fit according to Eq. 5 up to a maximum value of  $qR_g < 1.2$ .

$$\ln(I(q)) = \ln(I(0)) - \frac{1}{3} R_g^2 \cdot q^2 \quad (5)$$

For the model-dependent determination of the radius of gyration of the microgel particles (Fig. 7), a fuzzy-sphere model fit was performed, which is an extension of the homogeneous model with a smeared particle surface.

$$P(q) = \frac{3[\sin(qR) - qR \cos(qR)]}{(qR)^3} \exp\left(\frac{-(\sigma_{fuzzy}q)^2}{2}\right) \quad (6)$$

Here  $P(q)$  is the form factor,  $\sigma_{fuzzy}$  the fuzziness of the particle interface, and  $R$  represents the radius of the particle where the scattering length density profile decreases to 1/2 of the core density.

### Atomic force microscopy

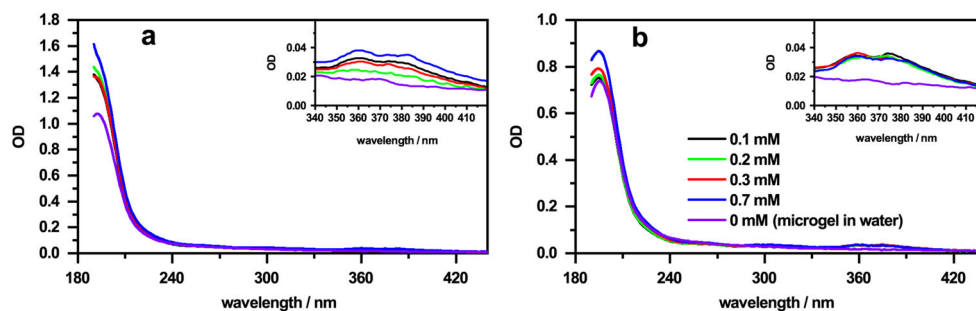
Atomic force microscopy was used to investigate the microgel particles for structural changes due to the addition of aescin. All measurements were performed on a FlexAFM (Nanosurf GmbH, Langen, Germany) in the dry state at room temperature in semi-contact mode using Al-Reflex Tap300Al-G cantilevers (Budget Sensors, Innovative Solution Bulgaria Ltd., Sofia, Bulgaria) with a tip radius of < 10 nm, a resonance frequency of about 300 kHz and a spring constant of 40 N/m. For the sample preparation a silicon wafer (Siegert Wafer GmbH, Aachen, Germany) was cleaned with ethanol (HPLC grade) and additionally in a plasma cleaner (Zepto, Diener Electronics, Ebhausen, Germany). Afterwards, the cleaned wafer was spin-coated with 0.1 mL of a PEI-solution (0.25 wt%) and of a highly diluted microgel suspension with and without aescin content. The samples were prepared as described for the UV/Vis measurements. The resulting images were analyzed with GWYDDION [50].

## Results and discussion

### Aescin uptake by PNIPAM and PNIPMAM microgels

In order to investigate whether the microgels used in this study take up the saponin aescin inside the polymer network

**Fig. 2** UV/Vis-spectra of PNIPAM (a) and PNIPMAM (b) microgels with different aescin amounts after centrifugation and redispersion in purified water. The measurements were performed at 20 °C in a wavelength range from 190 to 440 nm. The color code in (b) is also valid for (a) and gives the concentration of aescin in the solutions



or not, UV/Vis measurements were performed. Therefore, a defined amount of the microgels was mixed with aescin solutions of different concentrations. The resulting optical density at wavelengths around 190–420 nm is a superposition of the scattering process from the microgels and the absorption of light by aescin. The detected absorption will be used to quantify the uptake of aescin into the polymer network. After centrifugation and replacement of the supernatant by purified water, the spectra in Fig. 2 were obtained.

The spectrum (a) in Fig. 2 shows the change of optical density of PNIPAM due to the addition of different amounts of aescin. The solution of PNIPAM microgel particles without aescin exhibits an optical density of approx. 1.1 at a wavelength of 190 nm, resulting from the scattering processes by the microgel particles. By adding 0.1 mM (molar ratio = 0.006) aescin prior to the centrifugation, the optical density (OD) increases significantly to 1.4. Furthermore, an additional band appears in the region of 340–420 nm. This signal is characteristic for aescin and can also be found in the UV/Vis measurements of the residual aescin in the supernatant of the sample after centrifugation (see Fig. S1 in the supporting information (SI)) whereas an increase of the aescin amount to 0.2 mM (molar ratio = 0.012) does not induce a significant change in the OD after centrifugation. Increasing the aescin content further to 0.3 mM (molar ratio = 0.018) increases the OD again to a value of approx. 1.4. We suspect that aescin is initially stored homogeneously into the microgel interior due to the more hydrophobic character of PNIPAM compared with its environment, but the uptake seems to be somehow limited for these investigated concentrations. The aescin concentrations investigated correlate with aescins *cmc* and maybe incorporation of aescin into the microgel network becomes favored over the micelle formation of aescin in solution at these concentrations. The present experiments are performed in purified water and the solubility of aescin in pure water is decreased in comparison with a buffer solution. Consequently, this might lead to a decreased *cmc* value. If one now considers the band for the aescin concentration of 0.7 mM (molar ratio = 0.041), a sharp increase in the optical density to 1.6 can be recognized [51]. This indicates an increased storage rate of the saponin

at this particular concentration. Additionally, we suspect that at higher concentrations the incorporation takes place increasingly in the core of the particle due to the increased hydrophobicity in the core region caused by the previously homogeneously incorporated aescin molecules.

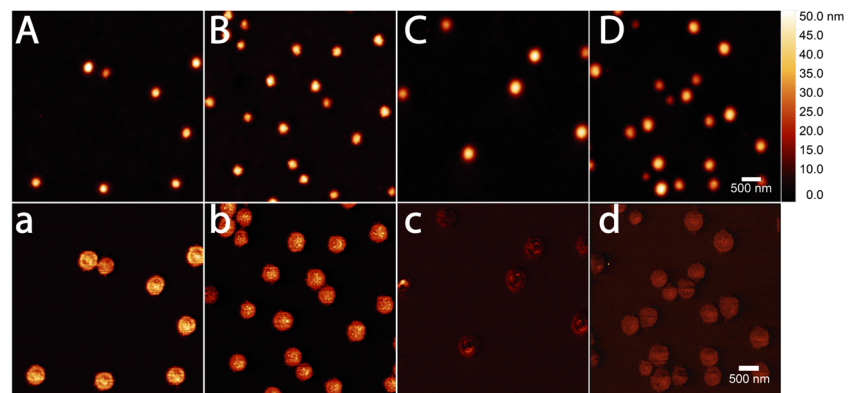
A similar trend can be observed for PNIPMAM microgels. The OD increases by increasing the aescin content in the solution which is used to swell the microgels. In contrast to PNIPAM particles, for PNIPMAM lower absolute values for the OD are obtained (see Fig. 2b). However, also the pure microgel solution of PNIPMAM shows a lower OD compared with the PNIPAM sample (0.7 to 1.1). Therefore, the decreased overall intensity can be assigned to a lower refractive index of the PNIPMAM solution. On the other hand, the increase of the OD by increasing the aescin content is much lower, which might also indicate a reduced uptake of aescin by PNIPMAM microgels compared with PNIPAM particles.

This becomes particularly clear when looking at the spectra for aescin concentrations of 0.1–0.3 mM. Compared with PNIPAM, at low-aescin concentrations, only a slight increase in optical density can be observed. This indicates a lower deposition of aescin in the microgel network. Only at an aescin concentration of 0.7 a significant increase in the OD to ca. 0.85 is observable. We suspect that due to the more hydrophilic nature of PNIPMAM and its distinctive cross-linker gradient compared with PNIPAM, the aescin incorporation rate into the polymer network is lowered, which causes the changes in OD to be rather small [52]. Only at higher aescin concentrations, a more homogeneous storage in the whole particle occurs, whereby the microgel becomes more compact, which leads to an increase in the OD.

To study the effect of aescin storage on the structure of the microgels used in this study, the microgel particles without and with 0.7 mM aescin present in the solution were also investigated by means of AFM. The obtained height images and the corresponding phase profiles are shown in Fig. 3 for both microgels.

Even at the first glance on the height images in Fig. 3, it can be seen that the PNIPAM microgels (A, B) are smaller than the PNIPMAM (C, D) particles. This explains the lower scattering and thus the lower optical density in

**Fig. 3** AFM images of PNIPAM microgels in water (**A, a**), and with 0.7 mM aescin (**B, b**) and PNIPAM microgels in water (**C, c**) and with 0.7 mM aescin (**D, d**). All measurements were performed in the dry state at room temperature. The height profiles are marked with a capital letter and the phase images with a lower case letter



the UV/Vis measurements for the PNIPAM microgels without aescin. Furthermore, the images clearly show particles with a spherical cross section in all cases for PNIPAM and PNIPMAM.

The phase image of PNIPAM without aescin (**a**) shows the typical core-corona structure for such microgels, where one observes a distinguished compact core and a rather fuzzy corona, representing the typical cross-linker gradient inside microgel particles [53, 54]. With the addition of 0.7 mM aescin to the microgel, the height image shows no difference at first sight (**B**). However, if the height profiles are extracted, a decrease in surface spreading compared to the microgel without aescin can be seen (see Fig. S2 in the SI). The particles contract slightly and therefore the height of the particles increases. Comparing the phase images of the microgel without aescin (**a**) and with aescin (**b**), it becomes obvious that the microgel with aescin shows a much less pronounced core-corona structure, which again illustrates the structural changes induced by the uptake of aescin molecules by the polymer network.

When looking at the height images of PNIPMAM without aescin and with aescin (**C, D**), no obvious differences are visible, similar to PNIPAM microgels. Again, the difference only shows when considering the height profiles (see Fig. S2 in the SI). Like for PNIPAM, the microgels with aescin become slightly more compact. However, this is less pronounced in the case of PNIPMAM. Furthermore, in contrast to PNIPAM, the height of the particles decreases slightly. Differences can also be observed in the phase images in panels (**c**) and (**d**). For PNIPMAM without aescin, as in case of PNIPAM, a classical core-corona structure can be recognized. If, however, the phase image of the microgel with aescin is considered, it can be seen once again that there is a phase difference between the core region and the particle exterior. The phase difference between the core region and the whole particle seems to be less strong, which supports the assumption that the aescin is deposited first in the core and then in the whole particle. Furthermore, a corona is recognizable here, which, however, is less pronounced

compared with the particles without aescin content. These results nicely match with the UV/Vis measurements.

### Influence of aescin uptake on the particle rigidity

After the investigation of the aescin uptake by UV/Vis spectroscopy and AFM imaging, we performed various light scattering experiments to gain insight into the particle diffusion and the structure of the microgels. In the following, the results from angle-dependent photon correlation spectroscopy (PCS) (see Figs. 4 and 5) are discussed. The measurements were performed for both

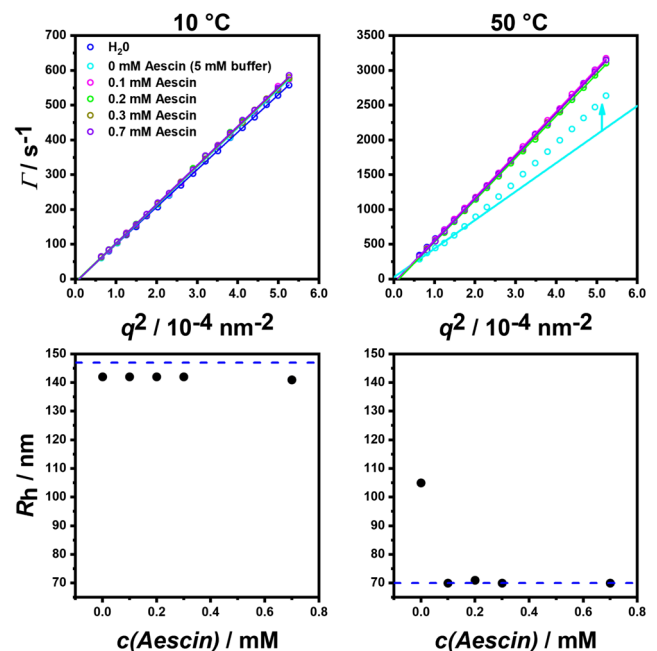


**Fig. 4** Top: Averaged relaxation rates  $\bar{\Gamma}$ , obtained by angle-dependent PCS, plotted against the square of the magnitude of the scattering vector  $q^2$  for PNIPAM microgels in presence of different aescin amounts (see figure legend) in the swollen (10 °C) and collapsed (50 °C) state. Straight lines represent linear fits for the determination of the hydrodynamic radius  $R_h$ . Bottom: Plots of the hydrodynamic radius  $R_h$  calculated from the slope of the  $\bar{\Gamma}$  vs.  $q^2$  plots in dependence of the present amount of aescin. The dotted blue lines represent the hydrodynamic radius of the microgel in deionized water (pH = 5.5)

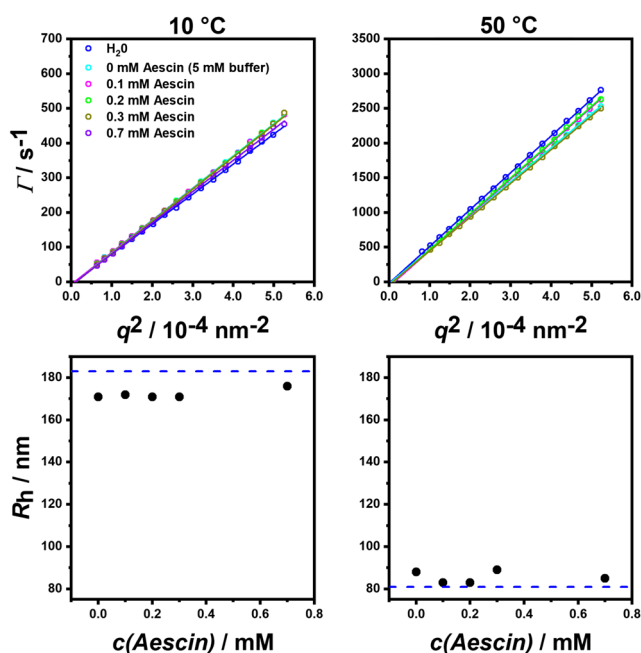


**Fig. 5** Top: Averaged relaxation rates  $\bar{\Gamma}$ , obtained by angle-dependent PCS, plotted against the square of the magnitude of the scattering vector  $q^2$  for PNIPAM microgels in presence of different aescin amounts (see figure legend) in the swollen (10 °C) and collapsed (50 °C) state. Straight lines represent linear fits for the determination of the hydrodynamic radius. Bottom: Plots of the hydrodynamic radius  $R_h$  calculated from the slope of the  $\bar{\Gamma}$  vs.  $q^2$  plots in dependence of the present amount of aescin. The dotted blue lines represent the hydrodynamic radius of the microgel in deionized water (pH = 5.5)

microgel systems in presence of different amounts of aescin, three below the *cmc* of aescin and one above the *cmc* of aescin as determined by Dargel et al. [38] (*cmc* = 0.35 mM). To obtain information about the temperature dependence of the systems, all measurements were performed in the swollen state (10 °C) and in the collapsed state (50 °C) of the microgel particles as well.

The plots of the mean relaxation rates of the PNIPAM microgels  $\bar{\Gamma}$  vs.  $q^2$  in the swollen state at 10 °C in Fig. 4 show the expected linear relation for all measured samples. As a quality check of the microgels, also measurements in water were performed and yielded a comparable result. Hence, it can be stated that the presence of aescin in the solution does not influence the particle diffusion behavior drastically. This is also visible if the hydrodynamic radii of the particles are calculated from the slope of the linear fits. The hydrodynamic radius of the PNIPAM particles in water is slightly higher, compared with the other measurements, but this can be assigned to the use of the 5 mM buffer solution. This buffer solution is used to increase the solubility of aescin. However, in all buffered solutions and in presence of all aescin concentrations, the hydrodynamic radius of the microgels is almost constant.

A very remarkable observation can be made, if the  $\bar{\Gamma}$  vs.  $q^2$  plots at high temperatures are investigated. While the microgel particles in water yield the expected linear relation of the mean relaxation rates and the square of the magnitude of the scattering vector, a significant difference is observed for the measurement in a 5 mM buffer solution. Here, the relaxation rate level off significantly from the expected linear trend (see blue arrow in Fig. 4). This behavior usually indicates the presence of aggregates in the microgel solution. This kind of aggregation of microgels at temperatures above the VPTT in presence of ions in the solution has been studied by Brian Vincent and co-workers [55, 56]. However, usually higher ionic strengths are necessary to cause a flocculation of the microgel particles though a calculation of the hydrodynamic radius of the dominant species is possible by using only the low  $q$ -values for the linear fit. Interestingly, the addition of aescin prevents the aggregation of the microgel particles, since the deviation from the expected linear behavior clearly disappears upon addition of aescin. This again points out the surfactant-like nature of aescin molecules, because comparable behavior has been found in previous studies, e.g., for sodium dodecyl sulfate [17]. These observations are confirmed if the hydrodynamic radius of the particles is calculated from the slope of the linear fits. While the calculated radius of the particles in buffer solution strongly exceeds the size of the collapsed microgel particle in water, the hydrodynamic radii obtained in presence of aescin are equal to the expected value.

Comparable with the previously mentioned experiments, similar measurements were performed for the second microgel species used in this work, namely PNIPMAM microgels. The results are displayed in Fig. 5.

As expected, the trends, observed for the PNIPAM microgels, are generally preserved in case of PNIPMAM. In the swollen state, aescin does not significantly influence the hydrodynamic properties of the microgel particles. Also, a comparable slight decrease in hydrodynamic radius in comparison with the measurements in water is observable here. In contrast to the PNIPAM microgels, a subsequent aggregation after increasing the measurement temperature is not observable for any of the samples. Maybe the smaller temperature difference between the VPTT of PNIPMAM and the measurement temperature causes this deviation in behavior of both systems. However, calculation of the hydrodynamic radii of all samples reveals once more that aescin does not strongly influence the hydrodynamic properties of the microgels.

In addition to PCS, we also performed static light scattering measurements. First, a model-independent analysis of the scattering data was performed to obtain insights into the structural properties of the microgel particles. Because of that, we decided to investigate the ratio of the radius of

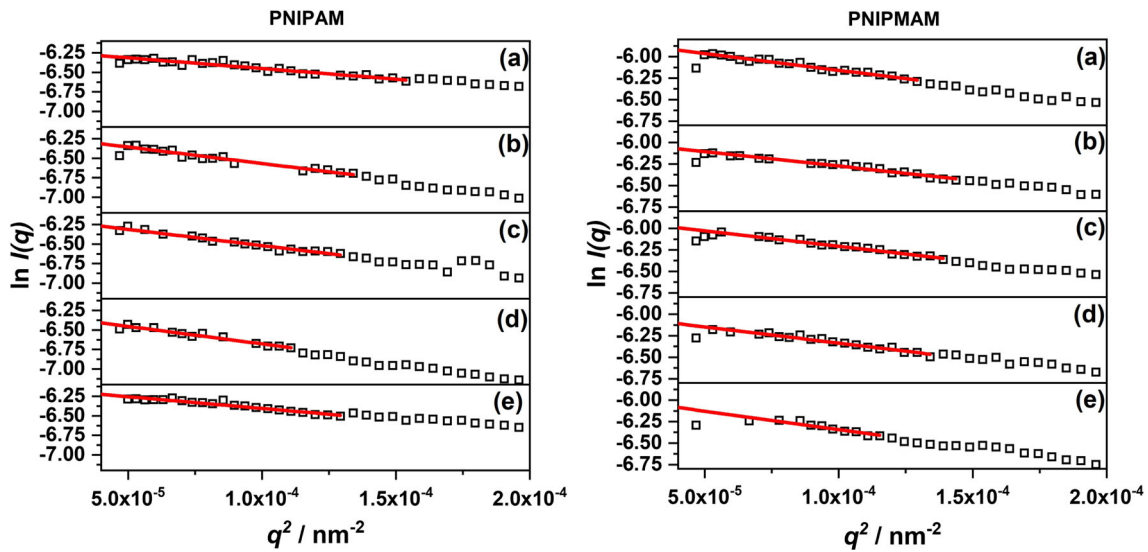


**Fig. 6** Guinier-plots for PNIPAM (left) and PNIPMAM (right) microgels in presence of 0 mM (a), 0.1 mM (b), 0.2 mM (c), 0.3 mM (d) and 0.7 mM (e) aescin. The red lines are linear fits used to obtain the radius

of gyration and the hydrodynamic radius of the particles ( $R_g/R_h$ ), which gives an idea of the general shape of the particles.

As depicted in Fig. 6a Guinier-analysis was possible for all microgels in the swollen state and the radius of gyration  $R_g$  could be determined from the slope of the plots. In contrast to previous methods, we observe rather strong differences between both types of microgels when performing the Guinier analysis and calculating  $R_g/R_h$  using the hydrodynamic radii, already obtained from angle-dependent PCS. All obtained values,  $R_g$ ,  $R_h$  and  $R_g/R_h$  are summarized in Table 1.

In case of the PNIPAM microgels, the initial  $R_g/R_h$  ratio is 0.62, a typical value for microgel particles indicating their fuzzy structure [57]. However, this value seems to be slightly too low, but this might be once again connected to the measurement in a buffer solution. Nevertheless, upon addition of aescin, the ratio strongly increases and reaches values in the region of 0.77 which is the theoretical value for a homogeneous sphere [58]. At very high aescin concentrations of 0.7 mM, the  $R_g/R_h$  decreases again, probably due to an increased incorporation in the now very hydrophobic core region of the microgel particle. However, the  $R_g/R_h$  ratio still does not reach the previous value of 0.62 obtained for the microgels without aescin addition.

A strong difference is observed for the same measurements in case of the PNIPMAM microgels. As expected for microgels, the initial  $R_g/R_h$  value is almost the same for the system without the addition of aescin. However, in case of the PNIPMAM microgels, the ratio of  $R_g/R_h$  decreases even more by the addition of aescin, indicating an even more pronounced core-corona structure usually

observed for copolymer microgels with very high amounts of charged comonomers like acrylic acid [59]. Upon addition of more aescin to the solution, the  $R_g/R_h$  ratio subsequently increases again eventually exceeding the initial value obtained for the pure microgel system in buffer, leading again to a very comparable result as exhibited by the PNIPAM microgels.

The previously described observations from the model-independent Guinier analysis seem to be very consistent with all other results, especially with those obtained from AFM. In addition to the Guinier analysis, also model-

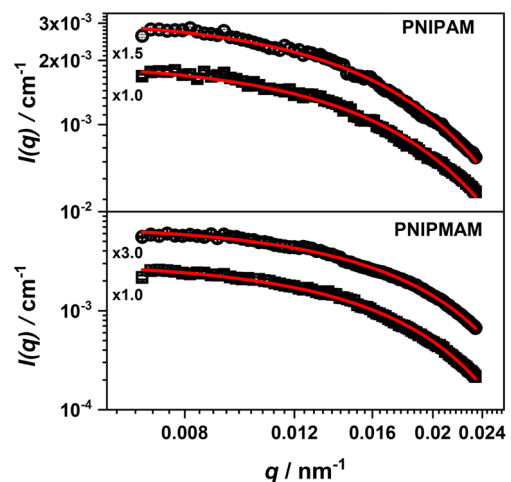


**Fig. 7** Form factor of PNIPAM (top) and PNIPMAM (bottom) microgels, measured in presence of 0 mM (squares, x1.0) and 0.7 mM (circles, x1.5) aescin with static light scattering. The straight red lines represent fits, obtained from the fuzzy-sphere model by fitting the data with the program SASFIT [60]. All measurements were performed at 10 °C in 5 mM phosphate buffer solution at pH = 7

**Table 1** Radius of gyration  $R_g$  (obtained from static light scattering), hydrodynamic radius  $R_h$  (obtained by angle-dependent PCS) and the ratio of both  $R_g/R_h$  for PNIPAM and PNIPMAM microgels in presence of all different amounts of aescin used in the present study

$c(\text{aescin}) / \text{mM}$	$R_g / \text{nm}$	$R_h / \text{nm}$	$R_g/R_h$
<b>PNIPAM</b>			
0	90 ± 4.5	142 ± 7.1	0.62 ± 0.05
0.1	112 ± 5.6	143 ± 7.1	0.78 ± 0.05
0.2	111 ± 5.5	142 ± 7.1	0.77 ± 0.05
0.3	115 ± 5.7	142 ± 7.1	0.80 ± 0.06
0.7	95 ± 4.7	141 ± 7.0	0.67 ± 0.05
<b>PNIPMAM</b>			
0	108 ± 5.4	171 ± 8.5	0.63 ± 0.05
0.1	100 ± 5.0	172 ± 8.6	0.57 ± 0.05
0.2	103 ± 5.1	171 ± 8.5	0.60 ± 0.05
0.3	106 ± 5.3	171 ± 8.5	0.62 ± 0.05
0.7	113 ± 5.6	171 ± 8.5	0.66 ± 0.05

dependent adaption was performed. Figure 7 shows the plot of  $I(q)$  as function of  $q$  for PNIPAM and PNIPMAM microgels in the swollen state (10 °C) in the buffer solution without aescin and in presence of 0.7 mM aescin. The data were fitted using the fuzzy sphere model. It is to mention that a model-dependent analysis, compared with the Guinier study (Table 1), is strongly dependent on the availability of features in the scattering curve.

Firstly, it is noticeable that the data from SLS measurements do not exhibit an observable form-factor minimum, due to the rather small size of the microgels. Of course, this makes the evaluation of the SLS data by fitting more complex and less reliable but nevertheless we performed a fit of the obtained data using the well-known fuzzy-sphere model introduced by Stieger et al. [20] (see Eq. 6). The results of the fitting procedure (displayed in Table 2) correlate very well with the observations we made in the dry state, using AFM and in the swollen state from the previous Guinier-analysis. In case of the PNIPAM microgels, the radius and polydispersity of the microgels are almost constant, while we observe a strong decrease in the parameter  $\sigma_{fuzzy}$ , which describes the expansion of the fuzzy shell surrounding the microgel particle, from around 12 to only 7 nm. This decrease in fuzziness is perfectly in line with the results we obtained from the analysis of the phase images of the microgels in AFM, where the mechanical properties of the particles changed to a more compact and homogeneous structure upon loading with aescin. A comparable effect is observable for PNIPMAM microgel particles, but in this case the compactization of the particle is less pronounced. Also, a change in the overall particle radius is visible, which has not been observed in case of the PNIPAM microgels. The same was true for the AFM measurements, where in

**Table 2** Results of the fuzzy-sphere model fits, obtained from SLS measurements for PNIPAM and PNIPMAM microgels in presence of 0 mM and 0.7 mM aescin (see Fig. 7)

$c(\text{aescin}) / \text{mM}$	$R / \text{nm}$	$\sigma_{fuzzy} / \text{nm}$	PDI
<b>PNIPAM</b>			
0	109 ± 2	12.2 ± 0.2	1.05 ± 0.02
0.7	108 ± 2	7.3 ± 0.06	1.05 ± 0.02
<b>PNIPMAM</b>			
0	140 ± 2	12.8 ± 0.7	1.04 ± 0.02
0.7	133 ± 2	10.2 ± 1.0	1.08 ± 0.03

contrast to the PNIPAM microgels still a core-corona structure was visible in the phase images, even after addition of aescin. We suggest that the less pronounced effect of the aescin on the particle structure of PNIPMAM microgels can be assigned to the lower amount of aescin incorporated inside the microgel network, which was revealed by the UV/Vis measurements.

We suspect that aescin is stored differently in the PNIPAM and PNIPMAM microgels due to the different cross-linker gradient. It would be possible that in PNIPAM microgels, in which this gradient is less pronounced, the aescin at low concentrations is initially embedded in the whole particle. At higher concentrations, the incorporation shifts to the core region due to the hydrophobicity in the particle interior, so that the aescin is finally distributed over the entire particle, which can also be seen in the AFM phase images and agrees well with the SLS results. In contrast, the cross-linker gradient is more pronounced in PNIPMAM microgels, which means that the core region of the particles is more hydrophobic in comparison to PNIPAM microgels. As a consequence, aescin is initially stored at low concentrations in the core region of the microgels and then in the outer area, whereby a certain corona still being present compared with PNIPAM microgels. However, even if AFM and SLS measurements support these assumptions, the particular process of the aescin incorporation and the origin of the interactions with the microgel network need to be explored in more detail in further studies.

### Influence of aescin uptake on the swelling behavior

In addition to the structural characterization of all samples, we performed temperature-dependent PCS measurements to record the swelling curves of the microgel particles in presence of aescin. In this context, it is particularly important, how the presence of aescin influences the VPTT of the microgel particles, since the possible release of aescin is supposed to be done by changing the temperature of the system. For this purpose, copolymer microgels with a defined VPTT above the body temperature would be

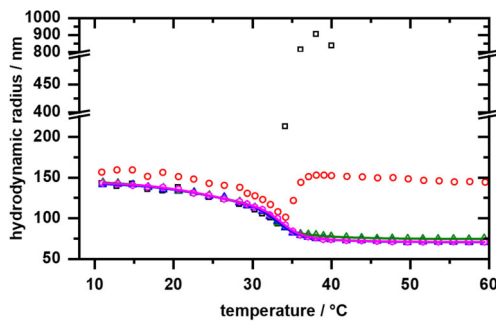


**Fig. 8** Temperature-dependent PCS measurements of PNIPAM microgels in presence of 0 mM (black squares), 0.1 mM (red circles), 0.2 mM (green triangles), 0.3 mM (blue triangles), and 0.7 mM (magenta diamonds) aescin. All measurements were performed in 5 mM buffer solution at pH = 7

suitable. The aescin-loaded microgels could be specifically targeted by hyperthermia, a common technique usually used as a complementary method in radiooncology, releasing aescin from the microgel network by the temperature induced collapse of the particles [61, 62]. However, first of all, it is important to understand how simple systems like PNIPAM and PNIPMAM behave by up-taking and releasing aescin. Hence, we particularly concentrate on the determination of the VPTT by a classical attempt to fit the swelling curves with a sigmoidal function and determine its point of inflection by derivation of this equation. This is at least a reasonable estimate for the phase transition temperature. For the sake of clarity, we will discuss the swelling curves of PNIPAM and PNIPMAM microgels separately in the following sub-subsections.

### PNIPAM microgels

The swelling curves of the PNIPAM microgels are displayed in Fig. 8. Just as a reminder, in the angle-dependent PCS measurements, we found a strong aggregation tendency of these microgels for the systems measured in buffer solution at 50 °C.

The analysis of the swelling curves of all PNIPAM microgel samples yields two important conclusions. Firstly, as expected, we observed a strong aggregation of the PNIPAM particles upon temperature increase. In line with the angle-dependent PCS measurements at high temperature, the addition of aescin prevents this aggregation, but contrary to the previous measurements, there still seems to be a certain amount of aggregation for the sample with 0.1 mM aescin in the solution. For higher amounts of aescin in the solution, the aggregation is completely suppressed as shown by the typical shape of the swelling curve as obtained from the PCS experiments.

The stabilization of the microgel particles is a very important effect of aescin in solution. Therefore, we

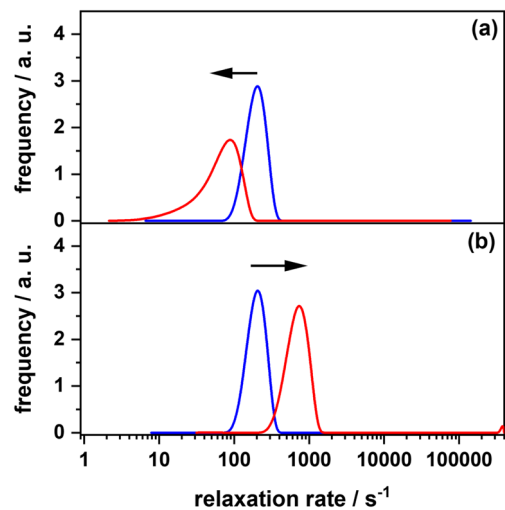


**Fig. 9** CONTIN-based relaxation rate distribution of PNIPAM microgels in pH = 7 buffer solution in presence of 0 mM (a) and 0.7 mM (b) aescin during the temperature-dependent PCS measurements at 10 °C (blue line) and 36 °C (red line)

performed a more detailed investigation by extracting the relaxation rate distribution of the microgels, from the PCS intensity correlation functions which were obtained by the CONTIN [49] algorithm, at 10 °C and 36 °C (see Fig. 9).

The relaxation rate distributions displayed in Fig. 9 nicely fits to the assumption of a strong stabilization of the microgel particles by the uptake of aescin molecules. By increasing the temperature, the mean relaxation rate in panel (a) switches to lower relaxation rates, connected to an increase in particle size, while the whole distribution becomes very broad and therefore indicates a high polydispersity of the system. It is also important that obviously no second particle species is observable at 36 °C, showing that the complete system is aggregated. Furthermore, a widening to very low relaxation rates and therefore huge sizes is observable, indicating a possible flocculation of the system.

This behavior obviously completely changes for the sample in presence of 0.7 mM aescin (panel (b)). In this panel, the mean relaxation rate changes towards faster relaxation rates upon increase of the temperature, representing a considerable decrease in particle size, while shape and intensity of the relaxation rate distribution stay more or less constant. Hence, aescin is indeed a stabilizing agent for PNIPAM particles, preventing their aggregation in the used buffer solution and helping to retain their initial polydispersity at high temperatures.

Of course, the planned fitting of the swelling curve with a sigmoidal function is not possible for the samples, which exhibit particle aggregation. As a compromise, we decided to use the onset of the aggregation as “VPTT” to determine a certain point in the graphs. In all other cases, the

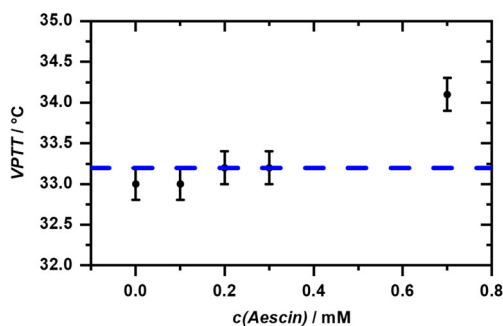


**Fig. 10** Evolution of the VPTT of PNIPAM microgels with increasing amount of aescin present in the solution. Due to the aggregation at low aescin concentrations the onset of aggregation was used as VPTT. Additionally, the VPTT of PNIPAM in aqueous solution was determined (blue dotted line, see SI)

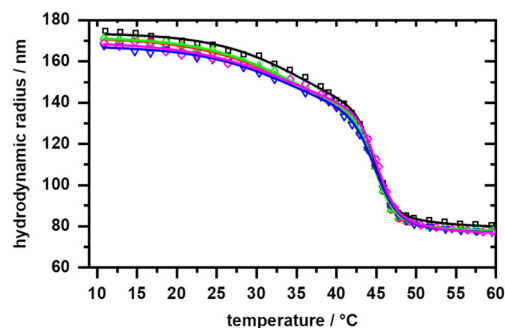
determination of the VPTT with our method was successful and yielded reliable results. Figure 10 shows the evolution of the VPTT upon increasing aescin concentration in the solution.

Figure 10 shows that a slight increase of the VPTT is observed with increasing amount of aescin in the solution. It was expected that aescin would act as a stabilizing agent for the microgel particles compared with the observations made previously for other surfactants. However, the increase in VPTT is still very small, even at the highest aescin concentration of 0.7 mM. This result strongly encourages the use of microgels as possible carrier systems for aescin, because even if a structural change in the network is observable due to the aescin incorporation, the swelling behavior stays unaffected and can therefore easily be predicted.

### PNIPMAM microgels

To complete the results on the swelling behavior of the microgel particles in presence of aescin, also all PNIPMAM samples were investigated by means of temperature-dependent PCS. The result can be found in Fig. 11.

Compared with the results of the PNIPAM microgels, the swelling curves of all PNIPMAM-based samples yield a rather simple result. For all concentrations of aescin, the swelling behavior of the PNIPMAM particles stays completely unaffected. This observation is strongly supported when the calculation of the VPTTs from the sigmoidal fits of the curves are performed. In case of our measurements, the VPTT of all samples is exactly 44.9 °C and therefore completely identical. This result seems to be in line with the reduced uptake of aescin inside the PNIPMAM particles, discussed in the other parts of this study. However, we also want to mention that PNIPMAM microgels generally exhibit a less pronounced response to the addition of surfactants concerning their VPTT and swelling behavior, which was already shown in



**Fig. 11** Temperature-dependent PCS measurements of PNIPMAM microgels in presence of 0 mM (black squares), 0.1 mM (red circles), 0.2 mM (green triangles), 0.3 mM (blue triangles), and 0.7 mM (magenta diamonds) aescin. All measurements were performed in 5 mM buffer solution at pH = 7

different studies, e. g., by Wedel et al. [63]. Furthermore, an additional look at the AFM and SLS results shows that both PNIPAM and PNIPMAM microgels have a certain corona without aescin content after the deposition of aescin. Although the microgel particles become more compact due to the incorporation of aescin and a shift of the VPTT would be expected, we suggest that it is precisely this corona and the so-called dangling ends that maintain the original VPTT of both systems.

### Aescin release

In the previous chapters, it has been shown that aescin can be successfully incorporated into the microgel network of PNIPAM and PNIPMAM. Following the uptake experiments, we also investigated the subsequent release of aescin from the microgel particles. Therefore, a defined amount of the microgels was mixed with an aescin solution of 0.7 mM (molar ratio = 0.016). The microgel-aescin mixtures were centrifuged at 10 °C. After the replacement of the first supernatant by purified water and repeated centrifugation, the second supernatant was investigated for aescin by UV/Vis spectroscopy. The same procedure was followed to study the release of aescin from the microgel network. However, to trigger the release of aescin, the microgel-aescin solution was heated to 50 °C during the second centrifugation step. The results are shown in Fig. 12.

The spectra (a) in Fig. 12 show the change of optical density depending on the released amount of aescin in the swollen (blue) and collapsed (red) state of PNIPAM. It can be seen that small amounts of aescin diffuse out of the microgel network in the swollen state. It is likely that the amount is even lower, as in this case forces are applied to the microgel during centrifuging whereby the particles are deformed, so probably larger amounts of aescin are kept within the network without centrifugation. By increasing the temperature above the VPTT, the microgel particles collapse,

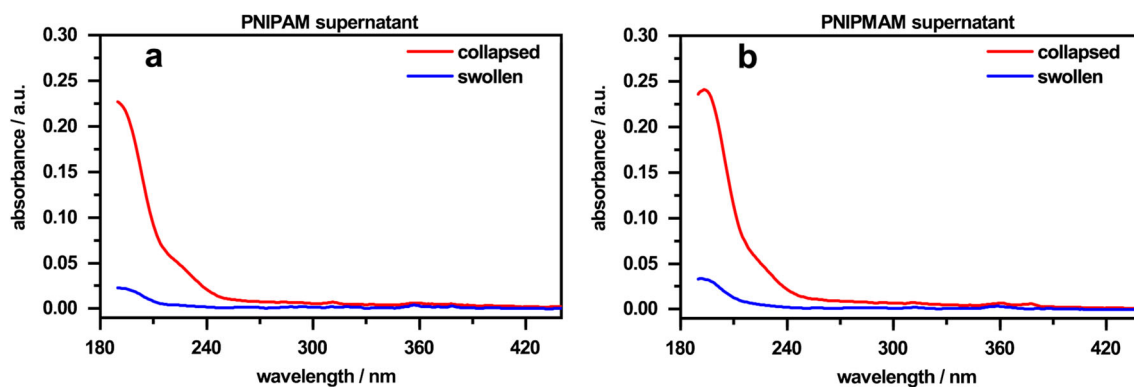


**Fig. 12** Absorbance spectra of the released aescin in the supernatants of PNIPAM (**a**) and PNIPMAM (**b**) microgels in the swollen (blue) and collapsed (red) state after two centrifugation steps and

replacement of the first supernatant by purified water. The measurements were performed at 20 °C in a wavelength range from 190 to 440 nm

releasing aescin from the network. This can be clearly recognized by the increase in the absorbance (red curve).

If these results are compared with the spectra for PNIPMAM (panel **(b)** in Fig. 12), it can be seen that, similar to PNIPAM, even in the swollen state, small quantities of aescin diffuse out of the network (blue curve). Furthermore, a slightly higher value for absorbance is visible, indicating that a larger amount of aescin is diffusing out of the microgel network. On the one hand, this can be attributed to the size of the particles, and on the other hand to the different uptake of aescin compared with PNIPAM microgels as shown before. After the deposition of aescin (0.7 mM) PNIPMAM shows still a fuzzy corona compared with PNIPAM. Since the network in the exterior of the particles is rather loose, we suspect that this may allow slightly more aescin to diffuse out of the particles in the swollen state, especially when additional forces during the centrifugation are applied. Nevertheless, if the curve for the triggered release (red) is considered, a clear increase in optical density can be seen just as in case of PNIPAM. Also, the amount of released aescin is comparable with the release in PNIPAM microgels.

In order to provide additional evidence that the change in the optical properties can be attributed to the release of aescin, the supernatants were investigated by means of electro-spray ionization mass spectrometry ESI-MS (see Fig. S4 in the SI). The analysis shows for both supernatants a characteristic molecular signal for aescin at  $m/z = 1129.3$ . This signal for aescin was also obtained by Dargel et al. [38] using electro-spray ionization high resolution mass spectrometry (ESI-HRMS) for the pure aescin compound.

## Conclusion

The main aim of this study was the examination of acrylamide-based microgels as carrier systems for the

natural surfactant aescin. Following that approach, we investigated the uptake of aescin into the network inside the particles and were able to show, e.g., by UV/Vis measurements, that aescin is indeed incorporated in the microgels. Also, particularly interesting results were yielded from atomic force microscopy and various light scattering experiments, where it was shown that aescin incorporation causes structural changes in the microgel architecture. These changes varied, when microgels based on PNIPAM or PNIPMAM were used as carrier systems, and surely the role of the chemical structure of the microgel particles in the uptake will remain a question to be investigated. Besides the structural changes identified in this study, we also investigated the swelling behavior of the microgel particles in presence of aescin and found only a very small change in the VPTT for PNIPAM-based microgels, while PNIPMAM particles remained completely unaffected by the presence of aescin in the solution. In the last part of this study, we could prove a successful release of aescin triggered by the collapse of PNIPAM and PNIPMAM microgels. Our results strongly encourage further investigations on these systems as possible drug delivery models. Copolymer microgels with a defined VPTT only slightly above the body temperature are of special relevance, since they would allow the use of hyperthermia [61, 62] already established in cancer treatment to release aescin. Furthermore, future studies might include the use of deuterated PNIPMAM and PNIPAM to perform contrast-matched small-angle neutron scattering experiments on microgels loaded with aescin to locate the aescin molecules inside the network [64] or the use of isothermal titration calorimetry to precisely determine the amount of aescin, which can adsorb in a microgel particle [65].

**Acknowledgments** Open Access funding provided by Projekt DEAL. Ina Ehring is gratefully acknowledged for her help with the PNIPMAM microgel synthesis.

**Funding information** The authors acknowledge financial support by the Deutsche Forschungsgemeinschaft (DFG) grant number HE2995/7-1.

## Compliance with ethical standards

**Conflict of interest** The authors declare that they have no conflict of interest.

**Open Access** This article is licensed under a Creative Commons Attribution 4.0 International License, which permits use, sharing, adaptation, distribution and reproduction in any medium or format, as long as you give appropriate credit to the original author(s) and the source, provide a link to the Creative Commons licence, and indicate if changes were made. The images or other third party material in this article are included in the article's Creative Commons licence, unless indicated otherwise in a credit line to the material. If material is not included in the article's Creative Commons licence and your intended use is not permitted by statutory regulation or exceeds the permitted use, you will need to obtain permission directly from the copyright holder. To view a copy of this licence, visit <http://creativecommons.org/licenses/by/4.0/>.

## References

- Saunders BR, Richtering W (2014) *Soft Matter*, pp 3695–3702. <https://doi.org/10.1039/c4sm00208c>
- Karg M, Pich A, Hellweg T, Hoare T, Lyon LA, Crassous JJ, Suzuki D, Gumerov RA, Schneider S, Potemkin II, Richtering W (2019) *Langmuir* 35(19):6231. <https://doi.org/10.1021/acs.langmuir.8b04304>
- Murthy N, Xu M, Schuck S, Kunisawa J, Shastri N, Frchet JMJ (2003) *PNAS* 100:4995. <https://doi.org/10.1073/pnas.0930644100>
- Schmaljohann D (2006) *Adv Drug Deliv Rev* 58(15):1655. <https://doi.org/10.1016/j.addr.2006.09.020>
- Zhang Y, Chan HF, Leong KW (2013) *Adv Drug Deliv Rev* 65(1):104. <https://doi.org/10.1016/j.addr.2012.10.003>
- Saunders BR, Laajam N, Daly E, Teow S, Hu X, Stepto R (2009) *Adv Colloid Interf Sci* 251:147–148. <https://doi.org/10.1016/j.cis.2008.08.008>
- Li X, Zhong H, Li X, Jia F, Cheng Z, Zhang L, Yin J, An L, Guo L (2014) *Materials Science & Engineering. C, Materials for Biological Applications* 45:170. <https://doi.org/10.1016/j.msec.2014.08.056>
- Hoffman AS (2002) *Advanced drug delivery reviews* 1(54). [https://doi.org/10.1016/S0169-409X\(01\)00239-3](https://doi.org/10.1016/S0169-409X(01)00239-3)
- Chen Y, Gao Y, da Silva LP, Pirraco RP, Ma M, Yang L, Reis RL, Chen J (2018) *Polym Chem* 9(29):4063. <https://doi.org/10.1039/C8PY00838H>
- Halacheva SS, Adlam DJ, Hendow EK, Freemont TJ, Hoyland J, Saunders BR (2014) *Biomacromolecules* 15(5):1814. <https://doi.org/10.1021/bm5002069>
- Hoare T, Pelton R (2008) *Langmuir* 24(3):1005. <https://doi.org/10.1021/la7024507>
- Jin X, Wang Q, Sun J, Panezail H, Wu X, Bai S (2017) *Polym Bull* 74(9):3619. <https://doi.org/10.1007/s00289-017-1915-4>
- Bradley M, Vincent B (2008) *Langmuir* 24(6):2421. <https://doi.org/10.1021/la703327v>
- Bradley M, Vincent B, Burnett G (2007) *Langmuir* 23(18):9237. <https://doi.org/10.1021/la701571w>
- Bradley M, Vincent B, Burnett G (2008) *Colloid Polym Sci* 287(3):345. <https://doi.org/10.1007/s00396-008-1978-8>
- Bradley M, Liu D, Keddie JL, Vincent B, Burnett G (2009) *Langmuir* 25(17):9677. <https://doi.org/10.1021/la900917v>
- Mears SJ, Deng Y, Cosgrove T, Pelton R (1997) *Langmuir* 13(7):1901. <https://doi.org/10.1021/la960515x>
- Tam KC, Ragaram S, Pelton RH (1994) *Langmuir* 10(2):418. <https://doi.org/10.1021/la00014a015>
- Pelton RH, Chibante P (1986) *Colloids Surf* 20(3):247. [https://doi.org/10.1016/0166-6622\(86\)80274-8](https://doi.org/10.1016/0166-6622(86)80274-8)
- Stieger M, Richtering W, Pedersen JS, Lindner P (2004) *J Chem Phys* 120(13):6197. <https://doi.org/10.1063/1.1665752>
- Pelton R (2000) *Adv Colloid Interf Sci* 85(1):1. [https://doi.org/10.1016/s0001-8686\(99\)00023-8](https://doi.org/10.1016/s0001-8686(99)00023-8)
- Wu C, Zhou S, Au-yeung SCF, Jiang S (1996) *Angew Makromol Chem* 240(1):123. <https://doi.org/10.1002/apmc.1996.052400111>
- Duracher D, Elaissari A, Pichot C (1999) *Colloid Polym Sci* 277(10):905. <https://doi.org/10.1007/s003960050470>
- Hosstettmann K, Marston A (1995) *Saponins*. Cambridge University Press. <https://doi.org/10.1017/cbo9780511565113>
- Vincken JP, Heng L, Groot AD, Gruppen H (2007) *Phytochemistry* 68(3):275. <https://doi.org/10.1016/j.phytochem.2006.10.008>
- Wilkinson JA, Brown AMG (1999) *Int J Cosmet Sci* 21(6):437. <https://doi.org/10.1046/j.1467-2494.1999.234192.x>
- Koh R, Tay I (2012) *Saponins: Properties, Applications and Health Benefits*. Nova Science Publishers Inc
- Francis G, Kerem Z, Makkar HPS, Becker K (2002) *Br J Nutr* 88(6):587. <https://doi.org/10.1079/bjn2002725>
- Tsibranska S, Ivanova A, Tcholakova S, Denkov N (2017) *Langmuir* 33(33):8330. <https://doi.org/10.1021/acs.langmuir.7b01719>
- Böttger S, Hofmann K, Melzig MF (2012) *Bioorg Med Chem* 20(9):2822. <https://doi.org/10.1016/j.bmc.2012.03.032>
- Golemanov K, Tcholakova S, Denkov N, Pelan E, Stoyanov SD (2013) *Soft Matter* 9(24):5738. <https://doi.org/10.1039/c3sm27950b>
- Matsuda H, Li Y, Murakami T, Ninomiya K, Yamahara J, Yoshikawa M (1997) *Biol Pharma Bull* 20(10):1092. <https://doi.org/10.1248/bpb.20.1092>
- Sirtori CR (2001) *Pharmacol Res* 44(3):183. <https://doi.org/10.1006/phrs.2001.0847>
- Lorent JH, Quetin-Leclercq J, Mingot-Leclercq MP (2014) *Org Biomol Chem* 12(44):8803. <https://doi.org/10.1039/c4ob01652a>
- Bangham AD, Home RW (1962) *Nature* 196(4858):952. <https://doi.org/10.1038/196952a0>
- Li B, Wang Z, Xie JM, Wang G, Qian LQ, Guan XM, Shen XP, Qin ZH, Shen GH, Li XQ, Gao QG (2019) *Acta pharmacologica Sinica* 40(1):111. <https://doi.org/10.1038/s41401-018-0001-2>
- Ming ZJ, Hu Y, Qiu YH, Cao L, Zhang XG (2010) *Phytomedicine: International Journal of Phytotherapy and Phytopharmacology* 17(8-9):575. <https://doi.org/10.1016/j.phymed.2009.12.009>
- Dargel C, Geisler R, Hannappel Y, Kemker I, Sewald N, Hellweg T (2019) *Colloids and Interfaces* 3(2):47. <https://doi.org/10.3390/colloids3020047>
- Sreij R, Prévost S, Dargel C, Dattani R, Hertle Y, Wrede O, Hellweg T (2018) *Mol Pharm* 15(10):4446. <https://doi.org/10.1021/acs.molpharmaceut.8b00421>
- Sreij R, Dargel C, Moleiro LH, Monroy F, Hellweg T (2017) *Langmuir* 33(43):12351. <https://doi.org/10.1021/acs.langmuir.7b02933>
- Sreij R, Dargel C, Schweins R, Prévost S, Dattani R, Hellweg T (2019) *Scientific reports*, 9(1). <https://doi.org/10.1038/s41598-019-41865-z>
- Sreij R, Dargel C, Hannappel Y, Jestin J, Prévost S, Dattani R, Wrede O, Hellweg T (2019) *Biochimica et Biophysica Acta (BBA) - Biomembranes* 1861(5):897. <https://doi.org/10.1016/j.bbamem.2019.01.015>

43. Sreij R, Dargel C, Geisler P, Hertle Y, Radulescu A, Pasini S, Perez J, Moleiro LH, Hellweg T (2018) *Phys Chem Chem Phys* 20(14):9070. <https://doi.org/10.1039/c7cp08027a>
44. Mazer NA, Benedek GB, Carey MC (1980) *Biochemistry* 19(4):601. <https://doi.org/10.1021/bi00545a001>
45. Small DM, Penkett SA, Chapman D (1969) *Biochimica et Biophysica Acta (BBA) - Lipids and Lipid Metabolism* 176(1):178. [https://doi.org/10.1016/0005-2760\(69\)90086-1](https://doi.org/10.1016/0005-2760(69)90086-1)
46. Hildebrand A, Neubert R, Garidel P, Blume A (2002) *Langmuir* 18(7):2836. <https://doi.org/10.1021/la011421c>
47. Geisler R, Dargel C, Hellweg T (2020) *Molecules* 25(1):117. <https://doi.org/10.3390/molecules25010117>
48. Koppel DE (1972) *J Chem Phys* 57:4814
49. Provencher SW (1982) *Comput Phys Commun* 27(3):229. [https://doi.org/10.1016/0010-4655\(82\)90174-6](https://doi.org/10.1016/0010-4655(82)90174-6)
50. Nečas D, Klapetek P (2012) *Open Phys* 10(1):99. <https://doi.org/10.2478/s11534-011-0096-2>
51. Wedel B, Hertle Y, Wrede O, Bookhold J, Hellweg T (2016) *Polymers* 8:162. <https://doi.org/10.3390/polym8040162>
52. Wrede O, Reimann Y, Lülsdorf S, Emmrich D, Schneider K, Schmid AJ, Zauser D, Hannappel Y, Beyer A, Schweins R, Götzhäuser A, Hellweg T, Sottmann T (2018) *Sci Rep* 8(1):13781. <https://doi.org/10.1038/s41598-018-31976-4>
53. Rudyak VY, Gavrilov AA, Kozhunova EY, Chertovich AV (2018) *Soft Matter* 14(15):2777. <https://doi.org/10.1039/c8sm00170g>
54. Wöll D, Hoppe Alvarez L, Eisold S, Gumerov RA, Strauch M, Rudov AA, Lenssen P, Merhof D, Potemkin II, Simon U (2019) *Nano letters*. <https://doi.org/10.1021/acs.nanolett.9b03688>
55. Rasmusson M, Routh A, Vincent B (2004) *Langmuir* 20(9):3536. <https://doi.org/10.1021/la049913n>
56. Rasmusson M, Vincent B (2004) *React Funct Polym* 58(3):203. <https://doi.org/10.1016/j.reactfunctpolym.2003.08.007>
57. Wiehemeier L, Brändel T, Hannappel Y, Kottke T, Hellweg T (2019) *Soft Matter* 15(28):5673. <https://doi.org/10.1039/c9sm00690g>
58. Kokufuta E, Ogawa K, Doi R, Kikuchi R, Farinato RS (2007) *J Phys Chem B* 111(29):8634. <https://doi.org/10.1021/jp070147d>
59. Hyatt JS, Douglas AM, Stanley C, Do C, Barker TH, Fernández-nieves A (2017) *Physical Review E*, 95(1). <https://doi.org/10.1103/physreve.95.012608>
60. Breßler I, Kohlbrecher J, Thünemann AF (2015) *J Appl Crystallogr* 48(5):1587. <https://doi.org/10.1107/s1600576715016544>
61. Hildebrandt B, Hegewisch-Becker S, Kerner T, Nierhaus A, Bakhshandeh-Bath A, Janni W, Zumschlinge R, Sommer H, Riess H, Wust P (2005) *International journal of hyperthermia: the official journal of European Society for Hyperthermic Oncology, North American Hyperthermia Group* 21(2):169. <https://doi.org/10.1080/02656730400003401>
62. Andocs G, Renner H, Balogh L, Fonyad L, Jakab C, Szasz A (2009) *Strahlentherapie und Onkologie : Organ der Deutschen Röntgengesellschaft... [et al.]* 185(2):120. <https://doi.org/10.1007/s00066-009-1903-1>
63. Wedel B, Brändel T, Bookhold J, Hellweg T (2017) *ACS Omega* 2(1):84. <https://doi.org/10.1021/acsomega.6b00424>
64. Gladman JM, Crowley TL, Schofield JD, Eaglesham A (1995) *Phys Scr* T57:146. <https://doi.org/10.1088/0031-8949/1995/t57/026>
65. Kimhi O, Bianco-peled H (2002) *Langmuir* 18(22):8587. <https://doi.org/10.1021/la025735r>

**Publisher's note** Springer Nature remains neutral with regard to jurisdictional claims in published maps and institutional affiliations.